Cement and Concrete Research 149 (2021) 106580

Contents lists available at ScienceDirect

Cement and Concrete Research

journal homepage: www.elsevier.com/locate/cemconres

Intrinsic self-stressing and low carbon Engineered Cementitious Composites (ECC) for improved sustainability

He Zhu [a], Duo Zhang [a], Tianyu Wang [a,b], Morgan McBain [a], Victor C. Li [a,*]

[a] Department of Civil and Environmental Engineering, University of Michigan, Ann Arbor, MI 48109, USA
[b] College of Engineering, China University of Geosciences-Wuhan, Wuhan, Hubei Province 430074, China

ARTICLE INFO

Keywords:
Engineered Cementitious Composites (ECC)
Limestone calcined clay cement (LC3)
Calcium sulphoaluminate cement (CSA)
Expansion
Shrinkage
Self-stress
CO2

ABSTRACT

Engineered Cementitious Composites (ECC) is an emerging cementitious composite material with ultra-high ductility. However, its higher cement dosage limits its material greenness and leads to concerns with drying shrinkage. In this research, an ECC utilizing limestone calcined clay cement (LC3) and calcium sulphoaluminate cement (CSA) is investigated, focusing on minimizing the material's embodied carbon while enhancing its durability with intrinsic self-stressing functionality. A self-stressing criterion is theoretically established and experimentally verified. X-ray diffraction patterns reveal an ettringite quantity that modulates the initial expansion and later expansion-reversal of LC3-CSA-ECC to support a persistent self-stressing mechanism. LC3-CSA-ECC has a lower (64%) carbon footprint and similar embodied energy compared to conventional concrete. When combined with the durability advantage (tiny crack, high ductility of 5.5%, and self-stressing function), this low carbon self-stressing ECC holds promise as a sustainable repair material that lowers the embodied and operational carbon in civil infrastructure.

1. Introduction

Developing countries, such as China and India, are experiencing rapid infrastructure development placing a huge demand on construction materials. With the advantages of good mechanical performance, flexibility in structural shaping, and local availability, concrete is one of the most used materials. Though the need for newly constructed infrastructures is lower in more developed countries (e.g. US), aging infrastructure often requires repeated repairs due to the brittle nature of concrete material [1,71], adding to global concrete consumption. In total, concrete consumption amounts to over 80% of total engineered material consumption by weight [2,3]. The production of cement accounts for 1.45 ± 0.20 billion tons of CO_2 emissions annually, ranking as the third-largest source of anthropogenic emissions [4]. Since cement serves as the most common binder in concrete, there is a significant concern regarding the embodied carbon of concrete materials. The vast quantities of concrete produced annually for new construction and infrastructure repair place significant pressure on the environment due to the high embodied and operational carbon [5]. Therefore, the development of sustainable materials that possess both low embodied carbon and are durable in field use is urgently needed.

Engineered Cementitious Composites (ECC) is a fiber-reinforced ductile concrete, exhibiting ultra-high tensile strain capacity (above 3%) and crack width control ability (below 0.1 mm) [6]. ECC has been established as a promising durable construction material in both structural and repair applications [6]. However, as required by micromechanics theory, coarse aggregate is eliminated from ECC to lower the matrix fracture toughness and meet the strain-hardening requirement. This change results in a high cement dosage [7,8] and a corresponding high carbon footprint for traditional ECC. Moreover, the high volume of cementitious materials with no coarse aggregate leads to a higher shrinkage, up to 1500–1800 με at 28 d comparing to 400–600 με for normal concrete [8,9]. This high shrinkage may lead to cracking under restraint conditions and jeopardize the structure's durability [10,11]. Therefore, the high carbon footprint and shrinkage of ECC remain a concern.

Shrinkage mitigation methods have been proposed for reducing the cracking risk in cementitious materials. The internal curing method, such as superabsorbent polymer (SAP) has been established in reducing autogenous shrinkage, but drying shrinkage is exacerbated [8]. Similar to the internal curing method, adoption of a water-repellent additive results in 50% lower shrinkage by blocking pore channels [11].

* Corresponding author.
E-mail addresses: zhuhe@umich.edu (H. Zhu), duzhang@umich.edu (D. Zhang), tiawang@umich.edu (T. Wang), mmcbain@umich.edu (M. McBain), vcli@umich.edu (V.C. Li).

https://doi.org/10.1016/j.cemconres.2021.106580
Received 5 April 2021; Received in revised form 25 June 2021; Accepted 12 August 2021
0008-8846/© 2021 Elsevier Ltd. All rights reserved.

Meanwhile, 60–70% of drying shrinkage reduction has been demonstrated in ECC by incorporating shrinkage reducing agent (SRA), however, concurrent with a strength reduction [12,13]. Moreover, a nearly zero-shrinkage ECC (200 με drying shrinkage at 28 d) has been developed by employing a low shrinkage composite cement [9].

In addition to low shrinkage ECC, expansive ECC has been developed by including expansive cement/agent in mixtures. ECC incorporating expansive cement/agent exhibits expansion at early age followed by loss of expansion at later age [14,15]. Due to the prominent creep effect at early age (before 3 days), up to 50% of expansive stress can be relaxed [16,17]. When combined with increasing stiffness and decreasing creep at later age, this expansive stress can reverse to a tensile stress as the expansion transitions to shrinkage. To eliminate the restrained tensile stress, a self-stressing ECC, which exerts pressure onto a restraining boundary, has been developed [8]. The self-stressing ECC tailored both the maximum expansion and the subsequent expansion loss by utilizing expansive cement and SRA. Self-stressing ECC [8] enhances the material durability; however, the addition of SRA increases the carbon footprint and material cost of ECC, which impedes its broader application.

The material greenness of ECC has been improved by replacing the ingredients with greener ones, such as substituting the ordinary Portland cement (OPC) with a high volume of fly ash (FA), using foundry green sand, and incorporating lower carbon fibers (such as replacing polyvinyl alcohol (PVA) fiber with polypropylene (PP) fiber) [6]. Specifically, the feasibility of adopting limestone calcined clay cement (LC3) in developing greener ECC has been demonstrated [7,18–20]. LC3 is a blended cement of limestone (LS), calcined clay, and OPC [4,7], with 20%–35% reduction in carbon emissions compared with OPC. It has been shown that the compressive strength of concrete with LC3 is comparable to that of OPC-based concrete. LC3-based concrete possesses enhanced durability due to a finer pore structure [4,19,21]. An LC3-based ECC shows a 33% reduced carbon footprint when compared to conventional OPC-based ECC [7,18].

No consensus about the effect of LC3 on shrinkage has been reached. The drying shrinkage of LC3 based concrete measured after 28 d was reported similar to that of OPC-based concrete [21]. A comparable autogenous shrinkage was also observed for LC3 and OPC-based concretes during the first 28 d [22]. However, a higher long-term autogenous shrinkage in LC3-concrete than in OPC-concrete was also reported [21]. Meanwhile, Nguyen et al. [23] suggested that LC3 increased the drying shrinkage, owing to higher pore size. Furthermore, Du and Pang [24] suggested that LC3 led to a higher chemical and autogenous shrinkage than OPC-concrete, attributing to the high pozzolanic reactivity. In contrast, a reduction of autogenous shrinkage was found when OPC was replaced with 50% volume of limestone [25]. The shrinkage/self-stressing performance of LC3-CSA based ECC has not been investigated in the literature.

The objective of this study is to enhance the sustainability of ECC via improving the material greenness and durability (self-stressing effect). To do so, different ratios of LC3-CSA blended cement were employed to tailor expansion and mechanical performance (especially the ductility). The free length change and restrained steel ring tests were employed to evaluate self-stressing performance. Compressive strength and uniaxial tests were conducted to measure mechanical properties. X-ray Diffraction (XRD) analysis was performed to understand the self-stressing mechanism. Finally, the carbon footprint of self-stressing ECC was evaluated.

2. Self-stressing criterion

Fig. 1 illustrates the typical free length change behavior of CSA-based ECC. A non-linear expansion is observed up to a time t_m followed by a more gradual contraction. Under boundary restraint, the restrained pressure (p) induced by the free length change (Fig. 1) at a given time (t_{m+n}) can be calculated based on the linear superposition principle (Eq. (1)).

$$p = \sum_{i=1}^{m} r_i \cdot E_i \cdot \frac{\varepsilon_{max}}{m} - \sum_{j=1}^{n} r_{m+j} \cdot E_{m+j} \cdot \frac{\varepsilon_{max} - \varepsilon'}{n} \quad (1)$$

where ε_{max} and ε' represent the maximum expansion and the length change at a given designated age when length deformation is considered stabilized. $\frac{\varepsilon_{max}}{m}$ and $\frac{\varepsilon_{max}-\varepsilon'}{n}$ are discrete deformation increments for time 0–t_m and t_m–t_{m+n}, respectively. r_i and r_{m+j} are the creep coefficient at time t_i and t_{m+j}; E_i and E_{m+j} denote the elastic moduli of ECC at time t_i and t_{m+j}. Eq. (1) can be simplified:

$$p = \overline{E_1}\varepsilon_{max} - \overline{E_2}(\varepsilon_{max} - \varepsilon') \quad (2)$$

$\overline{E_1} \equiv \sum_{i=1}^{m} \frac{r_i \cdot E_i}{m}$ is defined as an effective modulus, for the period (0-t_m); $\overline{E_2} \equiv \sum_{j=1}^{n} \frac{r_{m+j} \cdot E_{m+j}}{n}$ is defined as an effective modulus of ECC between t_m and designated age, such as 28 or 150 d. The effective moduli consider both the stiffness evolution and creep/relaxation effect. Self-stressing effect can be obtained when the magnitude of restrained interface pressure is positive. Therefore, a self-stressing function can be defined as Eq. (3).

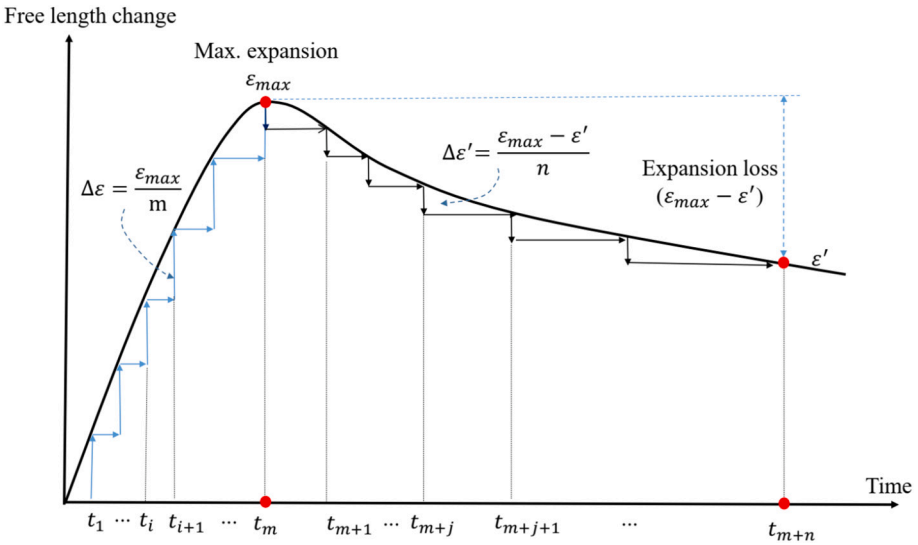

Fig. 1. Typical length change curve of CSA-based ECC [8].

$$\frac{f = \overline{E_1}}{\overline{E_2}\varepsilon_{max} - (\varepsilon_{max} - \varepsilon')} \quad (3)$$

A self-stressing criterion $f > 0$ represents a self-stressing effect, while $f \leq 0$ suggests no expansion pressure or tensile stress. The self-stressing criterion can be further expressed as Eq. (4)

$$\frac{\frac{(\varepsilon_{max} - \varepsilon')}{\varepsilon_{max}} < \overline{E_1}}{\overline{E_2}} \quad (4)$$

According to previous studies [8,15], the maximum initial expansion of CSA-based ECC is attained during the first days (0–3 d), which is further demonstrated in Section 4.1. During the initial expansion stage (0–t_1), the magnitude of $E_1(t)$ is small, while the creep effect is prominent, leading to a relatively small effective modulus ($\overline{E_1}$). With the development of elastic modulus and the weakened creep effect with age, $\overline{E_2}$ is always larger than $\overline{E_1}$. As demonstrated by restrained tests, the magnitude of effective moduli ratio ($\overline{E_1}/\overline{E_2}$) can range between 40% and 60%, depending on the material compositions and curing environment [10,17,26–28]. An average value of 50% of the effective moduli ratio is adopted as a plausible coefficient for predicting the self-stressing effect from the perspective of practical application. That is, the expansion loss should be controlled under 50% of its initial maximum expansion to obtain a robust self-stressing effect. The proposed criterion is further examined using the free length change and restrained expansion steel ring tests.

3. Experimental program

3.1. Materials and mix proportions

Three types of cement were employed to develop the intrinsic self-stressing Engineered Cementitious Composites (ECC), including Type I ordinary Portland cement (OPC), low carbon calcium sulphoaluminate cement (CSA), and limestone calcined clay cement (LC3). LC3 is a mix of OPC, metakaolin (MK), and limestone (LS) powder in a 55:30:15 weight ratio. Lower-cost less-pure calcined clays are commonly used in practice. Although MK and calcined clay have different morphology, size, and crystal phases, previous researchers have demonstrated that LC3-based concrete with lower-grade MK showed comparable mechanical and durability performance to those with high purity MK [29–32]. The high purity MK used in this study was based on laboratory availability to emulate the LC3. Fly ash (FA) was utilized for the dual purposes of enhancing ECC greenness and tailoring the matrix for a robust strain-hardening effect. Although limestone-calcined clay was originally proposed to mitigate the diminishing supply of conventional supplement cementitious materials [4], LC3 adopted in this study is treated as a greener cement working together with FA. FA has established benefits for high ductility in ECC. Tables 1 and 2 list the compositions of the binder ingredients (OPC, CSA, MK, LS, and FA), of which the particle size distribution and X-ray Diffraction (XRD) analysis can be found in a previous study [7].

All mixtures were prepared with a water to binder ratio of 0.3. Table 3 lists the proportions of used materials. The weight of FA was 2.2 times that of composite cement (the combinations of OPC, CSA, MK, and LS). A water reducer (WR) (Master Glenium 7920 from BASF) was used to obtain a 190 mm flow diameter per ASTM C1437 [33]. For OPC-based mixtures, 0%, 22%, 32%, and 42% weight of OPC were replaced by CSA, denoted as PC-C0, PC-C22, PC-C32, and PC-C42. For the LC3 series, LC3-C0, LC3-C22, LC3-C32, LC3-C42 represented that 0%, 22%, 32%, and 42% of the total cement was substituted by CSA, while the MK and LS maintained 30% and 15% weight ratio of the composite cement. 2% volume fraction of polypropylene (PP) fibers were employed to reinforce the matrix. The 12 μm diameter, 10 mm length PP fiber (Brasilit from Saint-Gobain Brazil) has 6 GPa Young's modulus and 850 MPa tensile strength.

The dry ingredients (OPC, CSA, MK, LS, FA) were pre-mixed for 10 min using a Hobart mixer (28.4-L volume). Then water associated with WR was added and further mixed for 5 min at 100 rpm to obtain a homogeneous paste. Finally, PP fibers (2% volume) were added to the fresh materials and mixed at 200 rpm for an additional 5 min. The fresh ECC was subsequently cast for the length change and mechanical tests.

The test protocols of ECC mixtures are described in the section below and summarized in Table 4.

Table 1
Oxide compositions determined by X-ray fluorescence of binder ingredients (%).

Oxide (%)	OPC	CSA	MK	LS	FA
CaO	63.5	47.2	0.0	54.8	17.4
Al_2O_3	4.8	10.1	46.6	–	19.8
SiO_2	19.6	7	50.8	0.2	39.4
Fe_2O_3	2.9	0.7	0.5	–	11
MgO	2.2	1.1	0.0	0.6	3.7
SO_3	2.6	33.1	0.1	–	1.9

Table 2
The phase composition of the OPC and CSA (mass %).

Anhydrous phase	Cement notation	OPC	CSA
Ye'elimite	$C_4A_3\overline{S}$		17.1
Alite	C_3S	62.6	
Belite	C_2S	14.4	25.2
Aluminate	C_3A	7.8	
Ferrite	C_4AF	9.3	0.9
Gypsum	$CaSO_4{\cdot}2H_2O$	2.9	5.1
Anhydrite	$CaSO_4$	1.4	39.9
Bassanite	$CaSO_4{\cdot}0.5H_2O$		12.4
Calcite	$CaCO_3$	6.6	

Table 3
Mix proportion of ECC matrix (kg/m^3).

Mixture	OPC	CSA	MK	LS	FA	Water	WR
PC-C0	490	–	–	–	1078	470	1.5
PC-C22	382	108	–	–	1078	470	1.5
PC-C32	333	157	–	–	1078	470	1.5
PC-C42	284	206	–	–	1078	470	1.5
LC3-C0	270	–	147	73	1078	470	4
LC3-C22	162	108	147	73	1078	470	4
LC3-C32	117	157	147	73	1078	470	4
LC3-C42	63	206	147	73	1078	470	4

3.2. Length change and mechanical performance tests

3.2.1. Free length change test

The free expansion/shrinkage test was performed according to ASTM C490/C490M–17 [34]. The specimens were cast into a 25 by 25 by 300-

Table 4
Test protocol of the ECC compositions.

Mixture	Free shrinkage/ expansion	Restrained steel ring	Tension	Compression	XRD[a]
PC-C0	X	–	X	X	X
PC-C22	X	–	X	X	–
PC-C32	X	–	X	X	–
PC-C42	X	X	X	X	X
LC3-C0	X	–	X	X	X
LC3-C22	X	–	X	X	–
LC3-C32	X	X	X	X	–
LC3-C42	X	X	X	X	X

[a] XRD samples were prepared from the paste material of ECC.

mm prism mold. The restrained stress started to build after setting, thus the final setting time was set as the initial time for measuring the free expansion/shrinkage after hardening [8]. The initial chemical/plastic shrinkage and ettringite expansion may be missed since they can start at a very beginning time. However, due to the negligible stiffness and the restrained effect of fibers, these initial deformations contribute little to the restrained stress [10,35–37]. While CSA accelerated the setting of composite cement, the final setting time per ASTM C403/C403M-16 [38] was 20 h for PC-C0 and LC3-C0; 10 h for PC-C22 and LC3-C22; 5.0 h for PC-32 and LC3-C32; 4.5 h for PC-C42 and LC3-C42, where the final setting time was also the earliest demolding time for measuring the free deformation without damaging the specimen. After demolding, the specimens were placed in a 20 ± 3 °C and 40 ± 5% RH environment for the free expansion/shrinkage test.

3.2.2. Restrained expansion ring test

While the restrained shrinkage steel ring has been widely used [26,39,40] for evaluating shrinkage-induced cracking, a restrained expansion steel ring was developed by Zhu et al. [8] to measure the expansion pressure. Fig. 2 shows the geometric dimension of the restrained expansion steel ring. In contrast to the hollow ring in the more common restrained shrinkage test, ECC (PC-C42, LC3-C32, and LC3-C42) mixes were solid cast inside the steel ring with 405 mm outer diameter, 385 mm inner diameter, and 150 mm height. The expansion of expansive ECC results in applied pressure against the steel ring, and the resulting strain of the steel ring was monitored by 3 strain gauges, starting 4.5 h after the cast and lasted for 28 d.

The residual interface pressure exerted by expansive ECC was calculated by Eq. (5) [41]:

$$p_{residual}(t) = \varepsilon_{steel}(t)E_{steel}\frac{\left(R_{Osteel}^2 - R_{Isteel}^2\right)}{2R_{Osteel}^2} \quad (5)$$

where $p_{residual}(t)$ is the residual interface pressure; $\varepsilon_{steel}(t)$ is the averaged strain measured by the three strain gauges; $E_{steel} = 210$ GPa is the Young's modulus of steel; $R_{Isteel} = 385\ mm$ and $R_{Osteel} = 405\ mm$ are the inner and outer diameters of the steel ring.

As discussed in Section 2, the expansive ECCs can exert pressure on the restrained ring when the ratio of expansion loss to initial maximum expansion is below 50%. Thus, only PC-C42, LC3-C32, and LC3-C42 in Table 4 which meet this requirement were examined by the restrained steel ring test, of which free length changes can be found in Section 4.1.

3.2.3. Chemical analysis (XRD)

LC3-C42 shows robust self-stressing performance (detailed in Section 4.2), so its hydration products, together with those of PC-C0, PC-C42, LC3-C0, were analyzed using the XRD method to determine the underlying mechanism. The paste samples were prepared with sealed plastic containers and tested on 0.5 d, 3 d, 28 d, and 150 d. After grinding the pastes into power to below 75 μm, the samples were analyzed using a Rigaku SmartLab high-resolution XRD (Cu-Kα radiation, 2θ-range 5–40°).

3.2.4. Compressive and uniaxial tensile test

After curing in air (20 ± 3 °C, 40 ± 5% RH) for 28 d, the 50 mm cubes and dogbone-shape specimens were used for compressive strength and uniaxial tension tests, where each test included 3 specimens per batch. Fig. 3 shows the dimension of the dogbone-shape specimen and the test setup. The uniaxial tension test was performed on an Instron servo-hydraulic system at a rate of 0.5 mm/min and with 80 mm gauge length measured by two linear variable displacement transducers (LVDT).

4. Results and discussions

4.1. Length change

The length change analysis suggests that LC3 based ECC has a reduced initial expansion peak, as well as a lower shrinkage reduction at later age when compared with OPC-based ECC. Fig. 4 shows the free length change results of OPC and LC3 based ECC with different CSA contents. In the absence of CSA cement, the drying shrinkage magnitude of LC3-C0 was approximately 70% that of PC-C0 after 28 d (Table 5). For example, LC3-C0 exhibited 1037 με of shrinkage at 28 d and 1434 με at 150 d, compared to that of 1434 με and 2087 με for PC-C0 at 28 d and 150 d, respectively. The capillary tensile stress caused by water loss from mesopores, of which the diameter is below a critical value of 25–50 nm, is the most widely accepted mechanism of drying shrinkage [2,42]. LC3-ECC was observed with a relatively coarser pore than OPC-ECC [18], where the binder system and water ratios were the same as the compositions herein. The coarser pore structure or the larger critical pore diameter of LC3-ECC reduces capillary tensile stress on capillary pores, leading to the observed lower drying shrinkage of LC3-C0 when compared with that of PC-C0.

The diminished drying shrinkage of LC3-ECC is consistent with that reported in the literature [25], where the cement was replaced by up to 50% weight of limestone. However, some contradictory results showing increased drying shrinkage in LC3 based concrete have also been reported [23,24]. Still others [20,21] have reported similar shrinkage magnitudes in LC3 and OPC-based concrete. The diverse findings may be attributed to different pore size distributions. For compositions with

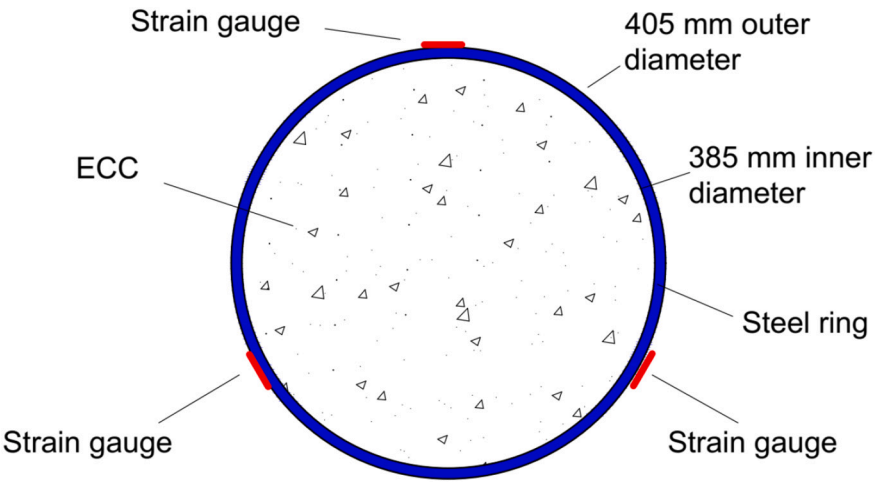

Fig. 2. Restrained expansion steel ring test setup.

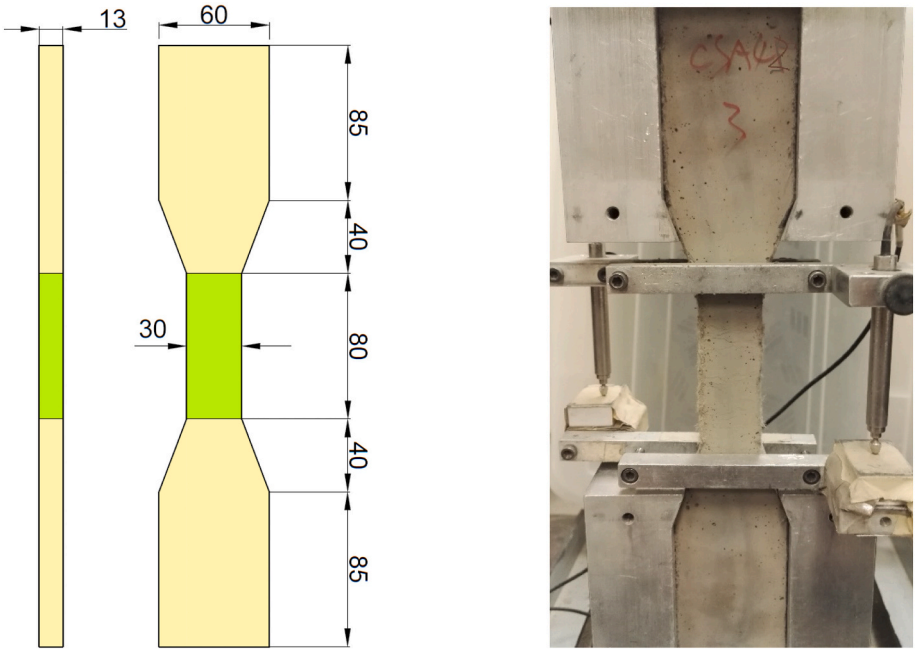

Fig. 3. The dimension of the dogbone-shape specimen. (Unit: mm).

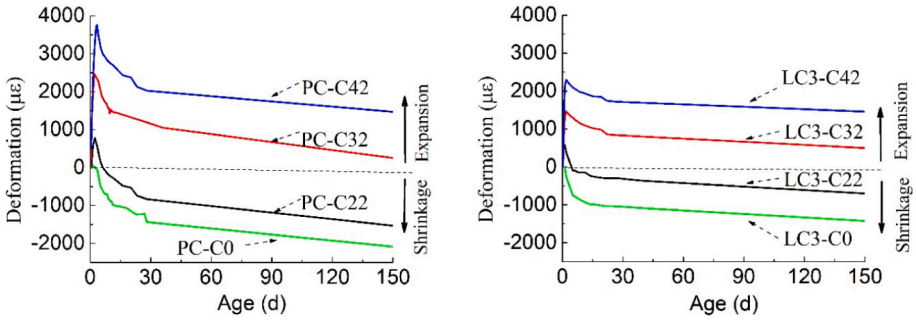

(a) OPC-based ECC (b) LC3-based ECC

Fig. 4. The free length change of ECC with different CSA addition ratios.

Table 5
Characteristic length change of LC3 and OPC-based ECC (με).

Mixture	Initial max. expansion	28 d	28 d-loss[b]	28 d-loss ratio[c]	150 d	150 d-loss[b]	150 d-loss ratio[c]
PC-C0	0	−1436[a]	−1436	–	−2087	−2087	–
PC-C22	780	−833	−1613	2.07	−1530	−2310	2.96
PC-C32	2468	1160	−1308	0.53	251	−2217	0.90
PC-C42	3756	2026	−1730	0.46	1469	−2287	0.61
LC3-C0	0	−1037	−1037	–	−1424	−1424	–
LC3-C22	579	−297	−876	1.51	−700	−1279	2.21
LC3-C32	1470	838	−632	0.43	500	−970	0.66
LC3-C42	2300	1722	−578	0.25	1459	−841	**0.37**[d]

[a] Positive and negative values indicate expansion and shrinkage, respectively.
[b] 28 d-loss = initial maximum expansion − 28 d-value; 150 d-loss = initial maximum expansion − 150 d-value.
[c] Loss ratio = −expansion loss/initial maximum expansion.
[d] Only LC3-C42 shows promise of long-term self-stressing effect.

sufficient OPC for hydration, LC3 based concrete can obtain a comparable or even higher compressive strength than OPC-based concrete because the high pozzolancity of calcined clay refines the pore microstructure, which also results in increased shrinkage. However, a high volume of FA is usually utilized in ECC composition to tailor the toughness of the matrix, where the FA accounts for 69% of the binder weight in this study. Further, the LC3 cement is blended by 55% OPC, 30% MK, and 15% LS in weight ratio, so the OPC only makes up 17% weight ratio in the entire binder system. The small OPC content generates less calcium hydroxide hydration product, depressing the hydration activity of MK and yielding a larger critical pore diameter as demonstrated by Zhu et al. [7] and Zhang et al. [18], which in turn accounts for the observed diminished shrinkage of LC3-C0 compared to PC-C0.

With increased CSA content, enlarged initial expansion is observed in

both OPC and LC3 based ECC. The initial expansion of LC3-C22 and LC3-C32 was roughly 60% of the PC-C22 and PC-C32, respectively. After reaching a peak, an expansion reversal/loss followed, leading to net shrinkage after 28 d for PC-C22 and LC3-C22. A critical replacement ratio of CSA to total cement existed, determining the long-term length change transition from shrinkage to expansion, in accordance with previous findings [15,8]. For example, both OPC and LC3 based ECC retained expansion after 150 d when the CSA replacement ratio exceeds 32%. Though LC3 based ECC had a lower initial expansion, comparable expansion values were observed at later age. For example, the 150 d expansion of LC3-C42 was 1459 με, compared to 1469 με for PC-C42. Additionally, the stable length change trend of LC3-ECC suggests a steady expansion for the long-term, while PC-C32 and PC-C42 maintain the contracting trend after 150 d.

4.2. Self-stressing verification

Following the self-stressing criterion described in Section 2, PC-C42, LC3-C32, and LC3-C42 were examined with the restrained steel ring test since their 28 d-expansion loss ratio was below 50%. The results of restrained expansion steel ring tests establish that LC3-C32 and LC-C42 possessed intrinsic self-stressing performance, while PC-C42 tended to be zero stress at 28 d. Similar to free length change, the steel strain showed expansion first and reversal subsequently (Fig. 5 (a)). Although PC-C42 retained 2026 με of free expansion at 28 d, the restrained expansion of the steel ring was nearly reduced to zero because the interface pressure development between steel ring and ECC results from the combined effects of creep and expansion deformation coupled with elastic modulus evolution of ECC with time. At early age (before 3 d), ECC has a relatively small elastic modulus and significant creep effect, resulting in relaxation of most of the interface stress [17,27] and in display of only 120 με of restrained strain. While the elastic modulus increases to a high level and the creep effect becomes insignificant at later age (e.g. 28 d), the expansion loss diminishes the restrained stress considerably. The noticeable expansion loss of PC-C42 at 28 d leads to the restrained ring strain (Fig. 5 (a)) and pressure (Fig. 5 (b)) decrease to zero. Although LC3-C32 and LC3-C42 showed moderate initial expansion and expansion loss magnitudes, their restrained pressure was maintained at 0.3–0.6 MPa at 28 d, suggesting an intrinsic self-stressing effect.

The proposed criterion in Eq. (4) is further verified by the restrained steel ring tests (Fig. 5). The 28 d-expansion loss ratio of PC-C42 is 0.46, indicating a low margin compared to 0.50. Consistent with this expectation, Fig. 5 (b) shows a low 0.06 MPa expansive pressure of PC-C42 at 28 d. The criterion (Eq. (4)) suggests that a lower expansion loss ratio results in retaining a higher residual pressure potential. In contrast, LC3-C32 and LC3-C42 maintain a low expansion loss ratio of 0.43 and 0.25, corresponding to an expected larger residual expansive pressure of 0.36 MPa and 0.55 MPa, respectively. The diminished expansive pressure at later age is caused by the relatively high elastic modulus and expansion loss compared to early age (such as 3 d earlier). Regarding the long-term self-stressing prediction, LC3-C42 has an expansion loss ratio at 150 d of 37%, while the expansion loss ratios of PC-C42 and LC3-C32 are higher than 0.6 (Table 5). This observation suggests that the self-stressing ability of LC3-C42 remains robust, while the expansive pressure of other mixtures will be eliminated by long-term shrinkage.

LC3 shows advantage over OPC in developing intrinsic self-stressing ECC. While the final length change retains expansion, the ratio of expansion loss to initial maximum expansion of LC3-ECC is significantly lower than that of OPC-ECC, which favors persistent expansive pressure. Although the long-term drying shrinkage of cementitious materials will be stable [9,44], the age of reaching the steady level is different among the tested compositions. Particularly, LC3-ECC shows a steady-state at 150 d compared to a slightly increasing trend for OPC-ECC, which is beneficial for the long-term self-stressing effect.

4.3. Mechanism of self-stressing effect

The XRD results (Fig. 6) suggest OPC-ECC pastes and LC3-ECC pastes have similar hydration products, including ettringite, portlandite (CH), and calcium silicates. Unhydrated ingredients, such as the calcite from limestone and the impurity quartz imported by FA, can be observed. Ettringite can be found in PC-C42 and LC3-C42 incorporating CSA. Though the expansion mechanism of CSA is not fully understood, the formation of ettringite [45,46] is widely accepted as the underlying cause. The presence of ettringite results in the initial expansion of PC-C42 and LC3-C42. The peak intensity of ettringite reaches a plateau at 3 d, corresponding to the time of maximum initial expansion for LC3-C42 and PC3-C42. More ettringite could be observed in PC-C42, accounting for the larger initial expansion of PC-C42 than that of LC3-C42.

The magnitude of the maximum initial expansion is determined by the hydration mechanism of CSA (Eqs. (6)–(8)), depending on the sulfate source and calcium hydroxide [46,47].

$$C_4A_3\overline{S} + 2C\overline{S}H_x + (38-2x)H \rightarrow C_3A\cdot 3C\overline{S}\cdot H_{12} + 2AH_3 \quad (6)$$

$$C_4A_3\overline{S} + (2+y)C\overline{S}H_x + yCH + \left(38 - x(2+y) + \frac{26}{3y}\right)H \rightarrow \left(1+\frac{y}{3}\right)C_3A\cdot 3C\overline{S}\cdot H_{12} + (2-y/3)AH_3 \quad (7)$$

$$C_4A_3\overline{S} + 18H \rightarrow C_3A\cdot C\overline{S}\cdot H_{12} + 2AH_3 \quad (8)$$

where $C_4A_3\overline{S}$, AH_3, $C_3A\cdot C\overline{S}\cdot H_{12}$, $C_3A\cdot 3C\overline{S}\cdot H_{12}$ represents ye'elimite, aluminum hydroxide, monosulfate, and ettringite. The sulfate source is expressed as $C\overline{S}H_x$, where x may be 0, 0.5, or 2, denoting the anhydrite, bassanite, and gypsum, respectively. CH refers to the hydration products portlandite and $y \in [0,6]$.

According to Fig. 6 (a), the quantity of CH increases with age for PC-

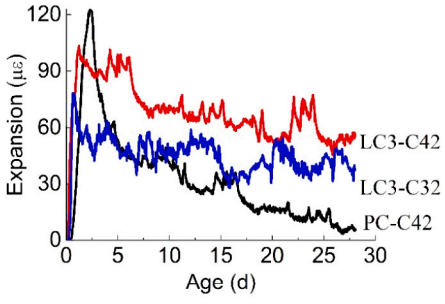

(a) Expansion of the steel ring.

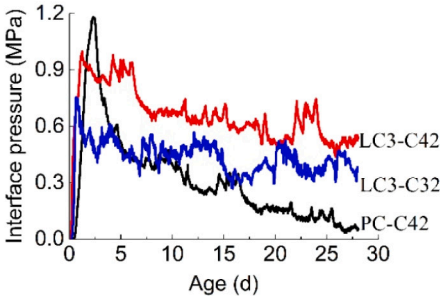

(b) Interface pressure between the ECC and the steel ring.

Fig. 5. Demonstration of self-stressing effect.

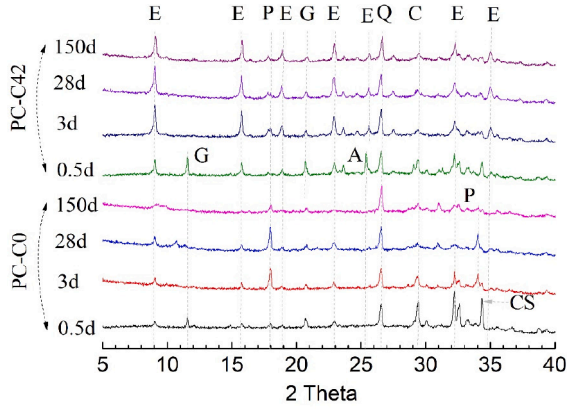

(a) XRD patterns of PC-C0 and PC-C42 at different ages (0.5-150 d).

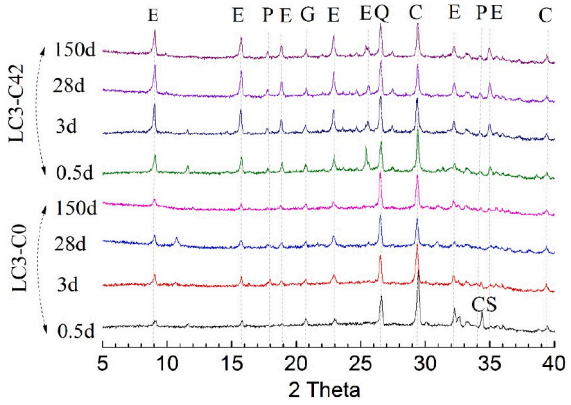

(b) XRD patterns of LC3-C0 and LC3-C42 at different ages (0.5-150 d).

Fig. 6. XRD patterns of the ECC pastes. (E: ettringite, P: portlandite (CH), G: gypsum, Q: quartz, C: calcite, CS: calcium silicates, A: anhydrite).

C0 (at least up to 28 d) but decreases with age for PC-C42. This suggests that the CH of PC-C42 is consumed following the reaction according to Eq. (7). Little CH is found in LC3-C0 hydration products (Fig. 6 (b)), suggesting that the main hydration of LC3-C42 follows Eq. (6). In the presence of CH (Eq. (7)), more ettringite is produced for the same volume of $C_4A_3\overline{S}$, accounting for the larger initial expansion of PC-C42 compared to LC3-C42.

The matrix strength and elastic modulus can influence the development of self-stressing behavior. Shen [48] observes that high strength matrix (>100 MPa) restrains the expansion of ettringite, however, this restrained effect is unremarkable for the low strength matrix (PC-C42 or LC3-C42) in this study, i.e., matrix strength plays an insignificant role in initial expansion compared to ettringite amount. By multiplying the higher initial expansion and elastic modulus [18], PC-C42 exhibits a higher initial expansive stress than LC3-C42 (Fig. 5 (b)). However, the higher elastic modulus combining with the later expansion reversal leads to a larger loss of expansive stress, rendering expansive stress of PC-C42 to tend to zero at 28 d (Fig. 5 (b)).

Ettringite decomposition is another mechanism accounting for the later expansion reversal. The gypsum is depleted for PC-C42 from 0.5 d to 150 d (Fig. 6 (a)), resulting in the formation of monosulfate after the consumption of $C\overline{S}H_x$ (Eq. (8)). This is consistent with the observed expansion loss (Table 5), where the 28 d and 150 d expansion loss increased slightly when CSA was incorporated. On the other hand, gypsum is observed in LC3-C42 (Fig. 6 (b)), indicating excess sulfate relative to ye'elimite for hydration with no concern for the transformation from ettringite to monosulfate. Additionally, the ettringite of LC3-C42 maintains a steady level from 3 d to 150 d (Fig. 6 (b)), suggesting negligible decomposition of ettringite in LC3-C42. Furthermore, limestone can react with calcium monosulfoaluminate to generate ettringite and calcium monocarboaluminate, improving the stability of ettringite [49,50]. Though the calcium monocarboaluminate is not observed in Fig. 6 (b) due to its low concentration [51], the stabilization of ettringite remains a plausible reason for the expansion loss reduction of LC3-C42 at 28/150 d with increasing CSA volume (Table 5).

The peak of ettringite of PC-C42 at 150 d is weaker than that at 3 d, indicating a possible dissolution of ettringite in PC-C42. However, the dissolution was not verified by the quantitative analysis in this study. ECC compositions (Table 3) include a large volume of amorphous FA (69% weight ratio of binder), decreasing the reliability of the quantitative analysis for ettringite using the XRD method [44], which needs further studies.

4.4. Mechanical performance

LC3-ECC shows a lower compressive strength (Fig. 7 (a)) and ultimate tensile strength (Fig. 7 (b)) than those of OPC-ECC at the same CSA content. For normal LC3-based concrete [21], calcined clay reacts with the CH and refines the pore structures, leading to a comparable or slightly higher strength to OPC-based concrete. However, for the ECC compositions in this study, the binder system consists of 69% FA and 31% cement, where OPC only accounts for 17% weight ratio in LC3-C0 and 4% in LC3-C42. Very few CH is generated in the hydration products as demonstrated in XRD results (Fig. 6), depressing the reaction activity of MK and contributing little to the strength improvement. The low OPC content in the ECC compositions is the reason for the diminished strength of LC3-ECC compared to OPC-ECC.

On the positive side, the tensile ductility improves remarkably from 3.7% (PC0) to 6.0% (LC3-C0), maintaining at 5.5% for the self-stressing ECC (LC3-C42). The inclusion of CSA enhances the compressive strength and ultimate tensile strength for both OPC and LC3 based ECC, while insignificantly affects the tensile strain capacity, as shown in the strain-hardening curves (Fig. 8). The enhanced tensile strain capacity of LC3-C0 and LC3-C42 is accompanied by multiple micro-cracking patterns (Fig. 9).

The crack patterns influence the durability of the repaired materials. When tensioned to 2% strain level, LC3-based ECC has a smaller crack width and crack spacing compared to those of OPC-based ECC (Table 6). The coefficient of permeability of ECC has been established to be related to the crack width and numbers [53,54]. The crack pattern of LC3-C42 at 2% level is comparable to that in Lepech [53] and Liu [54], where the coefficient of permeability was observed at 10^{-10} m/s magnitude, significantly lower than that of steel reinforcement mortar (10^{-6} m/s).

4.5. Material greenness

The carbon footprint and embodied energy of the self-stressing ECC were analyzed to quantify its environmental impacts. Table 7 lists the embodied energy and carbon footprint of the ECC ingredients. Utilization of greener ingredients is the main strategy for developing low carbon ECC, including OPC free cement (LC3, CSA, and geopolymer), supplement cementitious materials (FA, slags), aggregates (desert/river/sea/foundry sand), and fibers (PP/plant/polyethylene terephthalate (PET) fibers) [6,55–57]. Sand contributes 2–4% of the carbon emission in ECC compositions, playing an insignificant role in embodied CO_2 analysis [6]. While the ductility of PET-ECC and plant-ECC are low (below 1%), PP fiber remains a suitable alternative fiber for PVA [7,55,58]. Although the slag [59], rice husk ash [60], recycled fine powder [61], palm oil fuel ash [62] have been utilized for developing greener ECC, FA is one of the optimal supplement cementitious materials due to its mechanical performance and greenness advantages. The embodied energy and carbon of FA was not considered in the calculation because it was treated as waste material. The classic ECC mixture M45-ECC [63] and a regular concrete [7] were adopted as benchmarks, to demonstrate the low carbon advantage of self-stressing ECC. Table 8

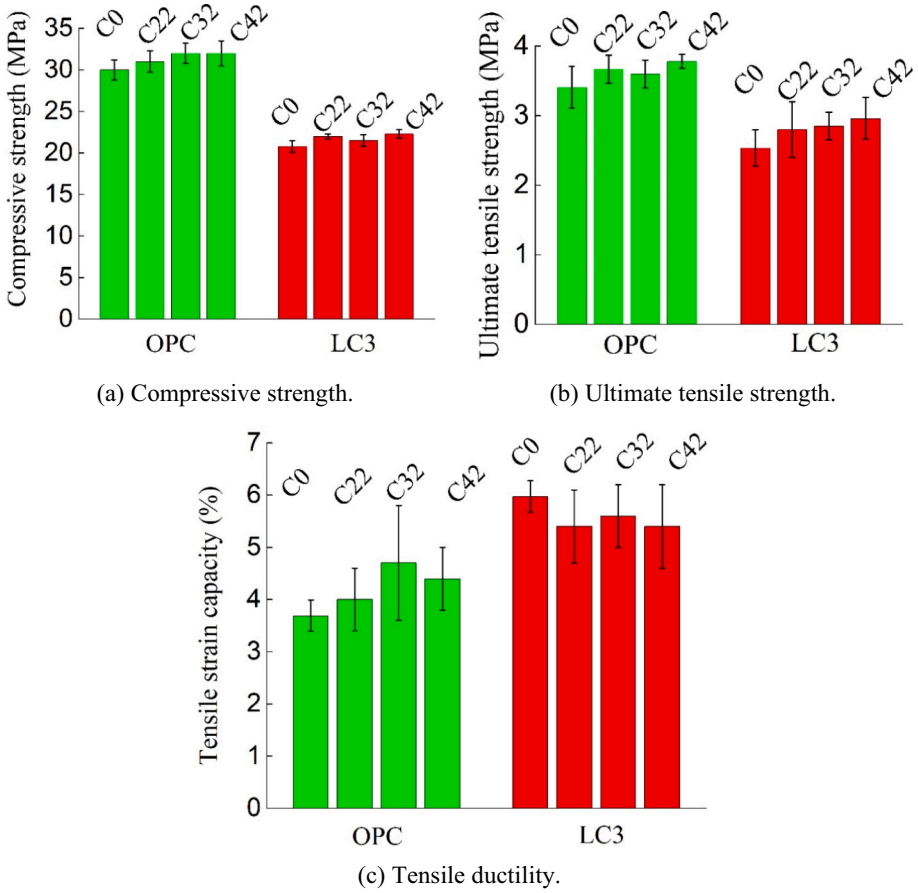

(a) Compressive strength. (b) Ultimate tensile strength.

(c) Tensile ductility.

Fig. 7. Mechanical performance of OPC-ECC and LC3-ECC with different CSA contents.

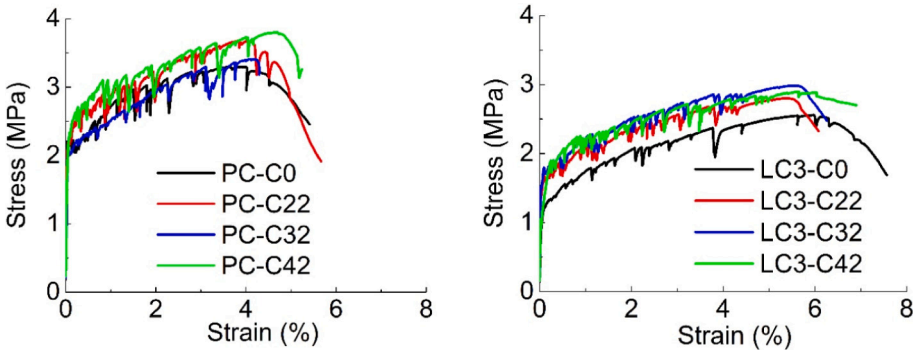

(a) OPC-ECC (b) LC3-ECC

Fig. 8. Tensile stress and strain curves of ECC with the different replacement ratios of CSA.

summarizes the material greenness and mechanical properties of the LC3-C42.

The carbon and energy footprints summarized in Fig. 10 suggest that use of cement accounts for most of the carbon emission and embodied energy, with fiber and chemical admixture contributing to the rest. The conventional M45-ECC shows a high carbon and energy intensity with 649 kg of carbon footprint and 6.4 GJ energy consumption (Table 8) for making 1 m^3 ECC. For the intrinsic self-stressing ECC (LC3-C42), the binder system is mainly composed of CSA, LS, MK, and FA, with only 4% OPC. As shown, CSA is a low carbon cement due to its low calcined temperature and grinding energy [67,68]. The combination of CSA and LC3 yields the 240 kg/m^3 carbon footprint of LC3-C42, corresponding to 64% that of conventional concrete. Further, even accounting for the embodied energy of the 2% PP fiber, the embodied energy of LC3-C42 (3.0 GJ/m^3) is comparable to that of conventional concrete (2.7 GJ/m^3). The developed LC3-C42 also show greenness advantages in comparison to previous technologies, such as the high volume of FA addition [66], geopolymer [57], etc.

In field repair applications, the intrinsic self-stressing effect and ultrahigh ductility of LC3-C42 enhance the durability of the repaired structure, leading to less maintenance or repair frequency. As established previously [69], the operational carbon associated with traffic detouring and congestion caused by repeated repair events during the use phase of transportation infrastructure can be substantially higher than the embodied carbon of the construction materials. Hence, the developed intrinsic self-stressing ECC represents a promising low life-

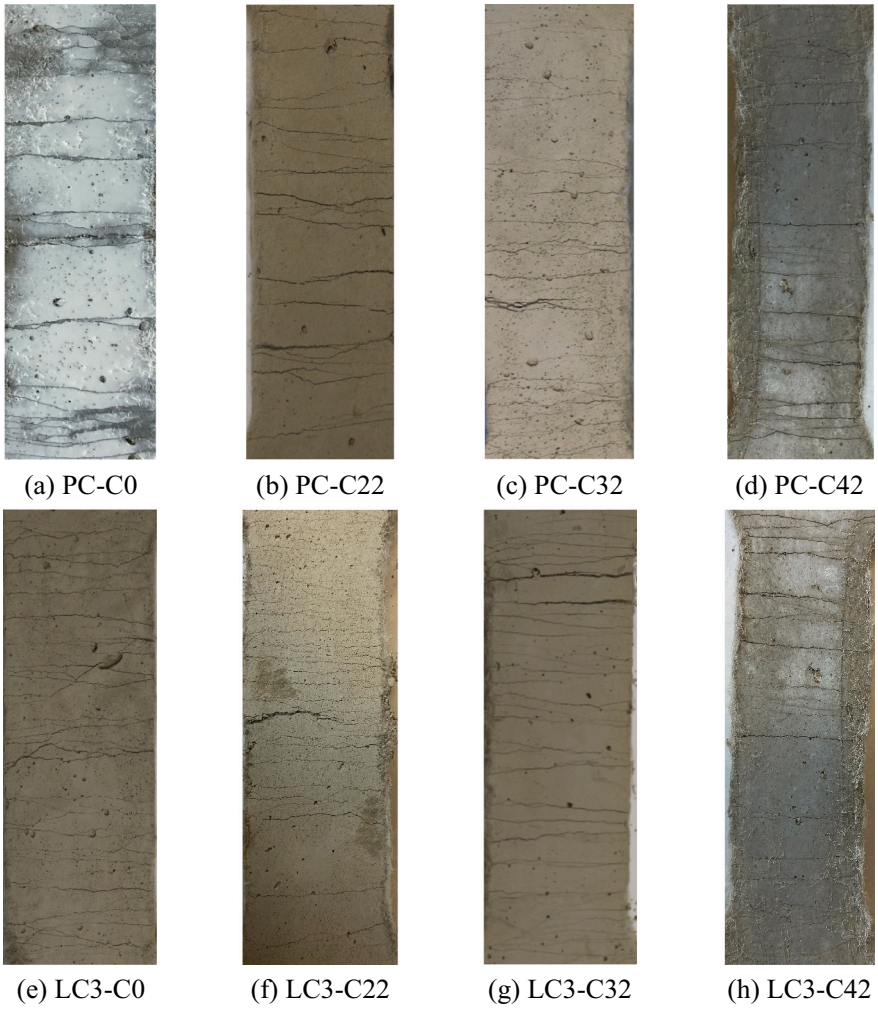

Fig. 9. Crack patterns of ECC specimens after direct tension tests.

Table 6
The characteristic crack parameters of ECCs at 2% strain and final failure.

Mixture		PC-				LC3-			
		C0	C22	C32	C42	C0	C22	C32	C42
2%	Crack number	15	18	21	19	25	23	20	23
	Crack width/μm	107	89	76	84	64	70	80	70
	Spacing/mm	5.3	4.4	3.8	4.2	3.2	3.5	4.0	3.5
Final crack	Crack number	22	26	28	27	37	34	33	32
	Crack width/μm	134	123	134	130	129	127	136	135
	Spacing/mm	3.6	3.1	2.9	3.0	2.2	2.4	2.4	2.5

Table 7
The embodied energy and carbon footprint of the ECC ingredients.

Index	OPC[a]	LCC[b]	CSA[c]	PP[a]	PVA[a]	Sand[a]	WR[d]
Energy (GJ/ton)	5.5	3.04	2.2	77.24	101	0.067	35
CO_2 (kg/ton)	900	210	360	3100	3400	23.3	1667

[a] Data from [7].
[b] LCC is a blend of limestone and calcined clay with a 1:2 weight ratio from [19]; the embodied CO_2 of pure MK and LS are 330 kg/ton [64] and 12.2 kg/ton [65], respectively, resulting in 224 kg/ton of CO_2 emission, which is comparable to that of LCC (210 kg/ton [19]).
[c] The energy and CO_2 of CSA are assumed to be 40% of OPC [45].
[d] Water reducer from [7].

Table 8
The greenness and mechanical properties of LC3-C42.

Mix. ID	Carbon footprint (kg/m^3)	Embodied energy (GJ/m^3)	Compressive strength (MPa)	Ultimate tensile strength (MPa)	Tensile strain capacity (%)
Concrete [66]	373	2.7	45	–	0.01
M45-ECC [63]	649	6.4	45	3.8	2.7
LC3-C42 ECC	240	3.0	23	3.0	5.5

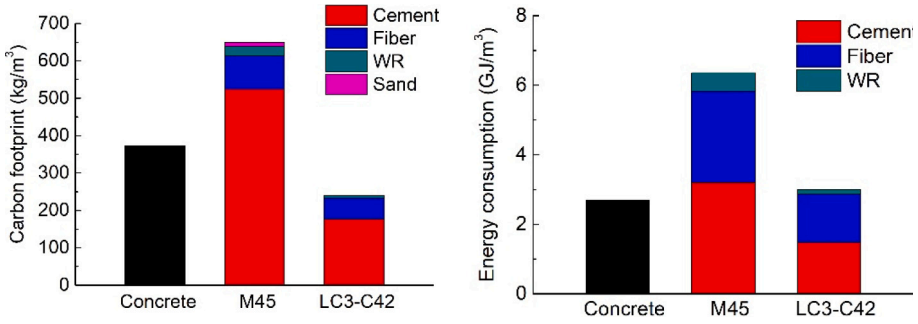

(a) Carbon footprint. (b) Embodied energy.

Fig. 10. Comparison of material greenness between the intrinsic self-stressing ECC and other benchmark concrete materials.

cycle carbon repair material for concrete infrastructure.

Although CSA is a greener alternative cement to OPC, CSA content should be chosen judiciously. As a rapid hardening cement, excessive amount of CSA will reduce working time. LC3-C42 adopts a moderate dosage of CSA (13% weight ratio of the binder). A sprayable LC3-C42 has been demonstrated with 80 min of operating time after adding water [70].

5. Conclusion

In this study, a ductile fiber reinforced cementitious composite with intrinsic self-stressing function has been developed and experimentally verified. Based on the findings from the length change test, restrained steel ring test, mechanical performance tests, XRD analysis, and material greenness analysis, the following conclusions can be drawn:

1. The proposed criterion of maintaining the self-stressing effect for restrained ECC is verified experimentally. Two requirements should be met to obtain a persistent self-stressing function: Firstly, the free length change of ECC must maintain expansion over time. Secondly, the ratio of expansion loss to initial maximum expansion should be lower than the effective moduli ratio (that includes the creep effect and age evolution) estimated as 0.5. The robust self-stressing function is confirmed based on an instrumented restrained steel ring test for mix composition (LC3-C42) that meets this criterion.
2. The strategy of combining CSA for expansion and LC3 for tailoring of initial maximum expansion and later expansion loss, is found to be effective for self-stressing function development. Without CSA, LC3-C0 has lower drying shrinkage compared to PC-C0. The drying shrinkage of LC3-based ECC reaches a steady state, while the OPC-based ECC retains a contracting trend after 150 d. With the inclusion of CSA, the free length change of ECC exhibits expansion first and expansion reversal subsequently. When cement is replaced with 42% of CSA, OPC-based ECC (PC-C42) shows a maximum expansion 1.6 times that of LC3 based ECC (LC3-C42). However, the later expansion loss of PC-C42 (2287 με) is substantially larger than that of LC3-C42 (841 με). The lower expansion loss ratio (0.37) of LC3-C42, as well as its low magnitude of long-term shrinkage, contribute to a persistent self-stressing.
3. Based on XRD patterns, it is confirmed that the quantity of ettringite is responsible for the differences in the observed time-dependent expansion behaviors of PC-C42 and LC3-C42. The presence of calcium hydroxide in PC-C42 hydrates promotes the formation of more ettringites, resulting in increased maximum expansion. However, at a later age, ettringite is more stable in LC3-C42 than in PC-C42 (such as 150 d) since limestone can suppress the transformation of ettringite to monosulfate. These findings reveal the mechanism underpinning the observed effectiveness of the self-stressing function in LC3-C42.
4. The 28 d compressive and ultimate tensile strength of LC3-C42 is 23% and 12% lower than those of the reference composition PC-C0. However, the tensile strain capacity of LC3-C42 is enhanced from 3.7% to 5.5% at 28 d. Also, the crack pattern of LC3-C42 is improved with lower crack width, more cracks, and smaller crack spacing, which suggest a lower permeability. The gain in ductility is more important than the loss of strengths, especially for a material designed for repair.
5. The developed self-stressing ECC (LC3-C42) is found to have a significantly lower carbon footprint than normal concrete and earlier versions of ECC materials. This has been achieved by incorporating low carbon CSA and LC3 cement in combination with low Portland cement content (4% of binder weight). The carbon footprint of LC3-C42 is 240 kg/m^3, corresponding to 64% that of conventional concrete (373 kg/m^3).

Despite having no coarse aggregates and with fiber reinforcement, LC3-C42 represents a durable repair material possessing persistent self-stressing function and low embodied carbon that supports durable and sustainable infrastructure renewal.

CRediT authorship contribution statement

He Zhu: Conceptualization, Methodology, Investigation, Formal analysis, Writing – original draft, Writing – review & editing. **Duo Zhang:** Data curation, Investigation, Writing – review & editing. **Tianyu Wang:** Investigation, Writing – review & editing. **Morgan McBain:** Data curation, Writing – review & editing. **Victor C. Li:** Funding acquisition, Project administration, Conceptualization, Writing – review & editing.

Declaration of competing interest

The authors declare that they have no known competing financial interests or personal relationships that could have appeared to influence the work reported in this paper.

Acknowledgments

This research is partially supported by the Center for Low Carbon Built-Environment (CLCBE) and the US Department of Energy, Advanced Research Projects Agency-Energy (ARPA-e) (Award number: DE-AR0001141) to the University of Michigan. The authors acknowledge the materials supply from BORAL RESOURCES (fly ash) and CTS Cement Manufacturing Corporation (CSA cement).

References

[1] ASCE, 2021 infrastructure report card. https://infrastructurereportcard.org/, 2021.

[2] P.K. Mehta, P.J.M. Monteiro, Concrete: Microstructure, Properties, and Materials, McGraw-Hill Education, 2014.
[3] M.F. Ashby, Materials and the Environment: Eco-informed Material Choice, 2nd ed., Elsevier, 2012.
[4] K. Scrivener, F. Martirena, S. Bishnoi, S. Maity, Calcined clay limestone cements (LC3), Cem. Concr. Res. 114 (2018) 49–56, https://doi.org/10.1016/j.cemconres.2017.08.017.
[5] P.K. Mehta, Global concrete industry sustainability, Concr. Int. 31 (2009) 45–48.
[6] V.C. Li, Engineered Cementitious Composites (ECC), Springer, 2019, https://doi.org/10.1007/978-3-662-58438-5.
[7] H. Zhu, D. Zhang, T. Wang, H. Wu, V.C. Li, Mechanical and self-healing behavior of low carbon engineered cementitious composites reinforced with PP-fibers, Constr. Build. Mater. 259 (2020), 119805, https://doi.org/10.1016/j.conbuildmat.2020.119805.
[8] H. Zhu, D. Zhang, Y. Wang, T. Wang, V.C. Li, Development of self-stressing Engineered Cementitious Composites (ECC), Cem. Concr. Compos. 118 (2021), 103936, https://doi.org/10.1016/j.cemconcomp.2021.103936.
[9] J. Zhang, C. Gong, Z. Guo, M. Zhang, Engineered cementitious composite with characteristic of low drying shrinkage, Cem. Concr. Res. 39 (2009) 303–312, https://doi.org/10.1016/j.cemconres.2008.11.012.
[10] H. Zhu, Y. Hu, Q. Li, R. Ma, Restrained cracking failure behavior of concrete due to temperature and shrinkage, Constr. Build. Mater. 244 (2020), https://doi.org/10.1016/j.conbuildmat.2020.118318.
[11] H. Zhu, Q. Li, R. Ma, L. Yang, Y. Hu, J. Zhang, Water-repellent additive that increases concrete cracking resistance in dry curing environments, Constr. Build. Mater. 249 (2020), https://doi.org/10.1016/j.conbuildmat.2020.118704.
[12] Y. Yang, Y. Yao, X. Gao, H. Deng, P. Yu, Shrinkage reducing measures for engineering cementitious composites, J. Wuhan Univ. Technol. Mater. Sci. Ed. 23 (2008) 907–911, https://doi.org/10.1007/s11595-007-6907-z.
[13] Y. Chen, J. Yao, Z. Lu, C.K.Y. Leung, Experimental study on the shrinkage reduction of high strength strain- hardening cementitious composites, Cem. Concr. Compos. 104 (2019), 103416, https://doi.org/10.1016/j.cemconcomp.2019.103416.
[14] A.K.F. Cheung, C.K.Y. Leung, Shrinkage reduction of high strength fiber reinforced cementitious composites (HSFRCC) with various water-to-binder ratios, Cem. Concr. Compos. 33 (2011) 661–667, https://doi.org/10.1016/j.cemconcomp.2011.03.009.
[15] W.C. Choi, H. Do Yun, Effect of expansive admixtures on the shrinkage and mechanical properties of high-performance fiber-reinforced cement composites, Sci. World J. 2013 (2013), https://doi.org/10.1155/2013/418734.
[16] H. Zhu, Y. Hu, Q. Li, M. Zhang, Determination of concrete elastic modulus in early age for temperature stress testing under the effect of restraint, in: S. Staquet, D. Aggelis (Eds.), Proc. 2nd Int. RILEM/COST Conf. Early Age Crack. Serv. Cem. Mater. Struct., RILEM Publications SARL, Brussels, 2017, pp. 603–608. https://www.rilem.net/publication/publication/529?id_papier=12726.
[17] H. Zhu, Q. Li, Y. Hu, R. Ma, Double feedback control method for determining early-age restrained creep of concrete using a temperature stress testing machine, Materials (Basel) 11 (2018), https://doi.org/10.3390/ma11071079.
[18] D. Zhang, B. Jaworska, H. Zhu, K. Dahlquist, V.C. Li, Engineered Cementitious Composites (ECC) with limestone calcined clay cement (LC3), Cem. Concr. Compos. 114 (2020), 103766, https://doi.org/10.1016/j.cemconcomp.2020.103766.
[19] J. Yu, H. Wu, C.K.Y. Leung, Feasibility of using ultrahigh-volume limestone-calcined clay blend to develop sustainable medium-strength Engineered Cementitious Composites (ECC), J. Clean. Prod. 262 (2020), 121343, https://doi.org/10.1016/j.jclepro.2020.121343.
[20] L. Wang, N. Ur Rehman, I. Curosu, Z. Zhu, M.A.B. Beigh, M. Liebscher, L. Chen, D. C.W. Tsang, S. Hempel, V. Mechtcherine, On the use of limestone calcined clay cement (LC3) in high-strength strain-hardening cement-based composites (HS-SHCC), Cem. Concr. Res. 144 (2021), 106421, https://doi.org/10.1016/j.cemconres.2021.106421.
[21] Y. Dhandapani, T. Sakthivel, M. Santhanam, R. Gettu, R.G. Pillai, Mechanical properties and durability performance of concretes with Limestone Calcined Clay Cement (LC3), Cem. Concr. Res. 107 (2018) 136–151, https://doi.org/10.1016/j.cemconres.2018.02.005.
[22] J. Ston, A. Hilaire, K. Scrivener, Autogenous shrinkage and creep of limestone and calcined clay based binders BT - calcined clays for sustainable concrete, in: F. Martirena, A. Favier, K. Scrivener (Eds.), Calcined Clays Sustain. Concr., Springer Netherlands, Dordrecht, 2018, pp. 447–454.
[23] Q.D. Nguyen, M.S.H. Khan, A. Castel, Engineering properties of limestone calcined clay concrete, J. Adv. Concr. Technol. 16 (2018) 343–357, https://doi.org/10.3151/jact.16.343.
[24] H. Du, S.D. Pang, High-performance concrete incorporating calcined kaolin clay and limestone as cement substitute, Constr. Build. Mater. 264 (2020), 120152, https://doi.org/10.1016/j.conbuildmat.2020.120152.
[25] S.-H. Kang, Y. Jeong, K.H. Tan, J. Moon, High-volume use of limestone in ultra-high performance fiber-reinforced concrete for reducing cement content and autogenous shrinkage, Constr. Build. Mater. 213 (2019) 292–305, https://doi.org/10.1016/j.conbuildmat.2019.04.091.
[26] H. Zhu, Y. Hu, R. Ma, J. Wang, Q. Li, Concrete thermal failure criteria, test method, and mechanism: a review, Constr. Build. Mater. 283 (2021), 122762, https://doi.org/10.1016/j.conbuildmat.2021.122762.
[27] S.A. Altoubat, D.A. Lange, Creep, shrinkage, and cracking of restrained concrete at early age, ACI Mater. J. 98 (2001) 323–331.
[28] Z. Zhao, K. Wang, D.A. Lange, H. Zhou, W. Wang, D. Zhu, Creep and thermal cracking of ultra-high volume fly ash mass concrete at early age, Cem. Concr. Compos. 99 (2019) 191–202, https://doi.org/10.1016/j.cemconcomp.2019.02.018.
[29] L.N. Assi, K. Carter, E. Deaver, P. Ziehl, Review of availability of source materials for geopolymer/sustainable concrete, J. Clean. Prod. 263 (2020), 121477, https://doi.org/10.1016/j.jclepro.2020.121477.
[30] F. Avet, K. Scrivener, Investigation of the calcined kaolinite content on the hydration of Limestone Calcined Clay Cement (LC3), Cem. Concr. Res. 107 (2018) 124–135, https://doi.org/10.1016/j.cemconres.2018.02.016.
[31] H. Maraghechi, F. Avet, H. Wong, H. Kamyab, K. Scrivener, Performance of Limestone Calcined Clay Cement (LC3) with various kaolinite contents with respect to chloride transport, Mater. Struct. Constr. 51 (2018) 1–17, https://doi.org/10.1617/s11527-018-1255-3.
[32] D. Zhao, R. Khoshnazar, Microstructure of cement paste incorporating high volume of low-grade metakaolin, Cem. Concr. Compos. 106 (2020), 103453, https://doi.org/10.1016/j.cemconcomp.2019.103453.
[33] ASTM C1437-15, Standard Test Method for Flow of Hydraulic Cement Mortar, ASTM International, West Conshohocken, PA, 2015. www.astm.org (n.d.).
[34] ASTM C490/C490M-17, Standard Practice for Use of Apparatus for the Determination of Length Change of Hardened Cement Paste, Mortar, and Concrete, ASTM International, West Conshohocken, PA, 2017. www.astm.org (n.d.).
[35] Z.P. Bažant, Prediction of concrete creep and shrinkage: past, present and future, Nucl. Eng. Des. 203 (2001) 27–38, https://doi.org/10.1016/S0029-5493(00)00299-5.
[36] W. Sun, H. Chen, X. Luo, H. Qian, The effect of hybrid fibers and expansive agent on the shrinkage and permeability of high-performance concrete, Cem. Concr. Res. 31 (2001) 595–601, https://doi.org/10.1016/S0008-8846(00)00479-8.
[37] A.Z. Bendimerad, E. Rozière, A. Loukili, Plastic shrinkage and cracking risk of recycled aggregates concrete, Constr. Build. Mater. 121 (2016) 733–745, https://doi.org/10.1016/j.conbuildmat.2016.06.056.
[38] ASTM C403/C403M-16, Standard Test Method for Time of Setting of Concrete Mixtures by Penetration Resistance, ASTM International, West, Conshohocken, PA, 2016 (n.d.).
[39] A.B. Hossain, J. Weiss, The role of specimen geometry and boundary conditions on stress development and cracking in the restrained ring test 36 (2006) 189–199, https://doi.org/10.1016/j.cemconres.2004.06.043.
[40] J.H. Moon, J. Weiss, Estimating residual stress in the restrained ring test under circumferential drying 28 (2006) 486–496, https://doi.org/10.1016/j.cemconcomp.2005.10.008.
[41] W.J. Weiss, W. Yang, S.P. Shah, Shrinkage cracking of restrained concrete slabs, J. Eng. Mech. 124 (1998) 765–774.
[42] F. Collins, J.G. Sanjayan, Effect of pore size distribution on drying shrinkage of alkali-activated slag concrete, Cem. Concr. Res. 30 (2000) 1401–1406, https://doi.org/10.1016/S0008-8846(00)00327-6.
[44] J.M. Abdalhmid, A.F. Ashour, T. Sheehan, Long-term drying shrinkage of self-compacting concrete: experimental and analytical investigations, Constr. Build. Mater. 202 (2019) 825–837, https://doi.org/10.1016/j.conbuildmat.2018.12.152.
[45] L.E. Burris, K.E. Kurtis, Influence of set retarding admixtures on calcium sulfoaluminate cement hydration and property development, Cem. Concr. Res. 104 (2018) 105–113, https://doi.org/10.1016/j.cemconres.2017.11.005.
[46] J. Bizzozero, C. Gosselin, K.L. Scrivener, Expansion mechanisms in calcium aluminate and sulfoaluminate systems with calcium sulfate, Cem. Concr. Res. 56 (2014) 190–202, https://doi.org/10.1016/j.cemconres.2013.11.011.
[47] S. Allevi, M. Marchi, F. Scotti, S. Bertini, C. Cosentino, Hydration of calcium sulphoaluminate clinker with additions of different calcium sulphate sources, Mater. Struct. Constr. 49 (2016) 453–466, https://doi.org/10.1617/s11527-014-0510-5.
[48] P. Shen, L. Lu, Y. He, F. Wang, J. Lu, H. Zheng, S. Hu, Investigation on expansion effect of the expansive agents in ultra-high performance concrete, Cem. Concr. Compos. 105 (2020), 103425, https://doi.org/10.1016/j.cemconcomp.2019.103425.
[49] L.H.J. Martin, F. Winnefeld, C.J. Müller, B. Lothenbach, Contribution of limestone to the hydration of calcium sulfoaluminate cement, Cem. Concr. Compos. 62 (2015) 204–211, https://doi.org/10.1016/j.cemconcomp.2015.07.005.
[50] Y. Zhang, X. Zhang, Research on effect of limestone and gypsum on C 3 A, C 3 S and PC clinker system 22 (2008) 1634–1642, https://doi.org/10.1016/j.conbuildmat.2007.06.013.
[51] L. Pelletier-chaignat, F. Winnefeld, B. Lothenbach, C. Jörg, Beneficial use of limestone filler with calcium sulphoaluminate cement, Constr. Build. Mater. 26 (2012) 619–627, https://doi.org/10.1016/j.conbuildmat.2011.06.065.
[53] M.D. Lepech, V.C. Li, Water permeability of engineered cementitious composites, Cem. Concr. Compos. 31 (2009) 744–753, https://doi.org/10.1016/j.cemconcomp.2009.07.002.
[54] H. Liu, Q. Zhang, C. Gu, H. Su, V.C. Li, Influence of micro-cracking on the permeability of engineered cementitious composites, Cem. Concr. Compos. 72 (2016) 104–113, https://doi.org/10.1016/j.cemconcomp.2016.05.016.
[55] J. Yu, J. Yao, X. Lin, H. Li, J.Y.K. Lam, C.K.Y. Leung, I.M.L. Sham, K. Shih, Tensile performance of sustainable Strain-Hardening Cementitious Composites with hybrid PVA and recycled PET fibers, Cem. Concr. Res. 107 (2018) 110–123, https://doi.org/10.1016/j.cemconres.2018.02.013.
[56] X. Huang, R. Ranade, W. Ni, V.C. Li, Development of green engineered cementitious composites using iron ore tailings as aggregates, Constr. Build. Mater. 44 (2013) 757–764, https://doi.org/10.1016/j.conbuildmat.2013.03.088.
[57] M. Ohno, V.C. Li, An integrated design method of Engineered Geopolymer Composite, Cem. Concr. Compos. 88 (2018) 73–85, https://doi.org/10.1016/j.cemconcomp.2018.02.001.

[58] D.G. Soltan, P. das Neves, A. Olvera, H. Savastano Junior, V.C. Li, Introducing a curauá fiber reinforced cement-based composite with strain-hardening behavior, Ind. Crop. Prod. 103 (2017) 1–12, https://doi.org/10.1016/j.indcrop.2017.03.016.
[59] M. Iqbal Khan, G. Fares, S. Mourad, Optimized fresh and hardened properties of strain hardening cementitious composites: effect of mineral admixtures, cementitious composition, size, and type of aggregates, J. Mater. Civ. Eng. 29 (2017), 04017178, https://doi.org/10.1061/(asce)mt.1943-5533.0002039.
[60] Z. Zhang, F. Yang, J.C. Liu, S. Wang, Eco-friendly high strength, high ductility engineered cementitious composites (ECC) with substitution of fly ash by rice husk ash, Cem. Concr. Res. 137 (2020), 106200, https://doi.org/10.1016/j.cemconres.2020.106200.
[61] K.Q. Yu, W.J. Zhu, Y. Ding, Z.D. Lu, J. tao Yu, J.Z. Xiao, Micro-structural and mechanical properties of ultra-high performance engineered cementitious composites (UHP-ECC) incorporation of recycled fine powder (RFP), Cem. Concr. Res. 124 (2019), 105813, https://doi.org/10.1016/j.cemconres.2019.105813.
[62] N.M. Altwair, M.A. Megat Johari, S.F. Saiyid Hashim, Flexural performance of green engineered cementitious composites containing high volume of palm oil fuel ash, Constr. Build. Mater. 37 (2012) 518–525, https://doi.org/10.1016/j.conbuildmat.2012.08.003.
[63] L. Kan, H. Shi, Investigation of self-healing behavior of Engineered Cementitious Composites (ECC) materials, Constr. Build. Mater. 29 (2012) 348–356, https://doi.org/10.1016/j.conbuildmat.2011.10.051.
[64] M.S. Meddah, M.A. Ismail, S. El-Gamal, H. Fitriani, Performances evaluation of binary concrete designed with silica fume and metakaolin, Constr. Build. Mater. 166 (2018) 400–412, https://doi.org/10.1016/j.conbuildmat.2018.01.138.
[65] S. Sánchez Berriel, A. Favier, E. Rosa Domínguez, I.R. Sánchez MacHado, U. Heierli, K. Scrivener, F. Martirena Hernández, G. Habert, Assessing the environmental and economic potential of Limestone Calcined Clay Cement in Cuba, J. Clean. Prod. 124 (2016) 361–369, https://doi.org/10.1016/j.jclepro.2016.02.125.
[66] J. Yu, S.M. Asce, C.K.Y. Leung, D. Ph, F. Asce, Strength improvement of strain-hardening cementitious composites with ultrahigh-volume fly ash 29 (2017), https://doi.org/10.1061/(ASCE)MT.1943-5533.0001987.
[67] M.C.G. Juenger, F. Winnefeld, J.L. Provis, J.H. Ideker, Advances in alternative cementitious binders, Cem. Concr. Res. 41 (2011) 1232–1243, https://doi.org/10.1016/j.cemconres.2010.11.012.
[68] Y. Lin, A.N. Scott, L. Wotherspoon, J. Ingham, Durability properties of sprayed engineered cementitious composite durability properties of sprayed engineered cementitious composite, ACI Mater. J. 110 (2013) 503–512.
[69] G.A. Keoleian, A. Kendall, J.E. Dettling, V.M. Smith, R.F. Chandler, M.D. Lepech, V. C. Li, Life cycle modeling of concrete bridge design: comparison of engineered cementitious composite link slabs and conventional steel expansion joints, J. Infrastruct. Syst. 11 (2005) 51–60, https://doi.org/10.1061/(asce)1076-0342(2005)11:1(51.
[70] H. Zhu, K. Yu, V.C. Li, Sprayable engineered cementitious composites (ECC) using calcined clay limestone cement (LC3) and PP fiber, Cem. Concr. Compos. 115 (2021), 103868, https://doi.org/10.1016/j.cemconcomp.2020.103868.
[71] He Zhu, Tianyu Wang, YiChao Wang, Victor. C Li, Trenchless rehabilitation for concrete pipelines of water infrastructure: A review from the structural perspective, Cement and Concrete Composites 123 (2021), 104193, https://doi.org/10.1016/j.cemconcomp.2021.104193.